Article

Deactivation of a single-site gold-on-carbon acetylene hydrochlorination catalyst: An X-ray absorption and inelastic neutron scattering study

Grazia Malta, Simon A. Kondrat, Simon J. Freakley, Catherine Davies, Simon Dawson, Xi Liu, Li Lu, Krzysztof Dymkowski, F Fernandez-Alonso, Sanghamitra Mukhopadhyay, Emma Kate Gibson, Peter P. Wells, Stewart F. Parker, Christopher J. Kiely, and Graham J. Hutchings

ACS Catal., **Just Accepted Manuscript** • DOI: 10.1021/acscatal.8b02232 • Publication Date (Web): 27 Jul 2018

Deactivation of a single-site gold-on-carbon acetylene hydrochlorination catalyst: An X-ray absorption and inelastic neutron scattering study

G. Malta[1], S. A. Kondrat[1,2], S. J. Freakley[1], C. J. Davies[1], S. Dawson[1], X. Liu[3], L. Lu[4], K. Dymkowski[5], F. Fernandez-Alonso[6,7], S. Mukhopadhyay[6,8], E. K. Gibson[9,10], P. P. Wells[11,12], S. F. Parker[6], C.J. Kiely[1,4], G.J Hutchings[1]*

1) Cardiff Catalysis Institute, School of Chemistry, Cardiff University, Main Building, Park Place, Cardiff, CF10 3AT, UK.

2) Department of Chemistry, Loughborough University, Loughborough, Leicestershire, LE113TU, U.K

3) SynCat@Beijing Synfuels China Co. Ltd., 1 Leyuan 2 South Street, Section C, Yanqi Economic Development Area, Beijing, 101407, China, P.R.

4) Department of Materials Science and Engineering, Lehigh University, 5 East Packer Avenue, Bethlehem, PA 18015, USA.

5) Scientific Computing Department, Rutherford Appleton Laboratory, Chilton, Didcot, Oxfordshire OX11 0QX, UK

6) ISIS Facility, STFC Rutherford Appleton Laboratory, Chilton, Didcot, Oxon OX11 0QX, UK.

7) Department of Physics and Astronomy, University College London, Gower Street, London WC1E 6BT, UK

8) Department of Materials, Imperial College London, Exhibition Road, London SW7 2AZ, UK

9) UK Catalysis Hub, Research Complex at Harwell, RAL, Oxford, OX11 0FA, UK.

10) School of Chemistry, Joseph Black Building, University of Glasgow, Glasgow G12 8QQ, U.K.

11) School of Chemistry, University of Southampton, Southampton, SO17 1BJ, U.K.

12) Diamond Light Source, Harwell Science and Innovation Campus, Chilton, Didcot OX11 0DE, UK.

*Hutch@Cardiff.ac.uk

ABSTRACT: Single-site Au species supported on carbon have been shown to be the active sites for acetylene hydrochlorination. The evolution of these single-site species has been monitored by Au L_3 X-ray Absorption Spectroscopy (XAS). Alternating between a standard reaction mixture of HCl/C_2H_2 and the single reactants, has provided insights into the reaction mechanism and catalyst deactivation processes. We demonstrate that oxidative addition of HCl across an Au(I) chloride species requires concerted addition with C_2H_2, in accordance with both the XAS measurements of Au oxidation state and the reaction kinetics being 1st order with respect to each reactant. The addition of excess C_2H_2 changes the Au speciation and results in the formation of oligomeric acetylene species which were detected by inelastic neutron scattering. Catalyst deactivation at extended reaction times can be correlated with the formation of metallic Au particles. The presence of this Au(0) species generated during the sequential gas experiments or after prolonged reaction times, results in the analysis of the normalized near edge white line intensity of the Au L_3 X-ray absorption spectrum alone becoming an unsuitable guide for identifying the active Au species, affecting the strong correlation between normalized white line height and VCM productivity usually observed in the active catalyst. Thus, a combination of scanning transmission electron microscopy and detailed modelling of whole XAS spectrum was required to distinguish active Au(I) and Au(III) species from the spectator Au(0) component.

KEYWORDS: Acetylene hydrochlorination, gold catalysis, heterogeneous catalysis, single-site catalysis, deactivation

INTRODUCTION

Vinyl chloride monomer (VCM) is a large scale chemical intermediate used almost exclusively as a precursor to polyvinyl chloride (PVC). Annually over 13 million tons of VCM are produced by acetylene hydrochlorination. Traditionally, acetylene hydrochlorination has been catalysed using mercuric chloride supported on high surface area activated carbon. While this catalyst is highly active and has been industrially employed for several decades, it is extremely volatile and highly toxic.[1,2,3,4] Following the prediction of Hutchings in 1985 that Au would be an effective catalyst for the reaction based on a correlation with electron affinity,[5] Au supported on carbon has recently been validated as a replacement catalyst for this large scale industrial process.[6]

The preparation method for making the Au/C catalysts has been demonstrated to strongly influence the corresponding structure and activity of the catalyst.[7,8,9] Active catalysts were prepared by the impregnation of $HAuCl_4$ onto C in strongly oxidising solutions of nitric acid or aqua regia, while it was found that using an aqueous $HAuCl_4$ solution produced catalysts with low activity. Characterization of these catalysts by a range of techniques, including X-ray photoelectron spectroscopy (XPS) and scanning transmission electron microscopy (STEM), suggested that the active catalysts had high Au dispersion and contained both oxidised Au(III) and Au(I) species. While these catalyst structure-activity studies revealed the importance of cationic Au species, the exact distribution of oxidation states and their chemical nature proved difficult to determine. Firstly, XPS and STEM analyses can easily alter the relative distributions of Au(0), Au(I) and Au(III) species and can induce the formation of nanoparticles in the samples through beam modification [10,11,12,13,14,15] Secondly, the reaction occurs under an aggressive chemical environment which can cause dynamic changes to the catalyst structure during reaction.

Recently, we reported the first detailed *in situ* X-ray absorption spectroscopy characterization study following the behaviour of these Au/C catalysts during the acetylene hydrochlorination reaction.[9] Analysis of the Au L_3-edge X-ray absorption near edge structure (XANES) and the extended X-ray absorption fine structure (EXAFS) showed the operating catalyst comprised of atomically dispersed cationic species, with no Au nanoparticles being present in the most active Au/C catalysts. During the reaction, distinct changes in the XANES were observed, which clearly correlated to the catalyst productivity, showing that the active catalysts were comprised of atomically dispersed cationic gold in both Au(III) and Au(I) oxidation states. While this provided new details of the nature of the active catalyst under operating conditions, we reason that studying the deactivation of the catalyst will provide a more profound understanding of the catalytic behaviour and the reaction mechanism to generate the information needed to design catalysts that exhibit extended lifetimes under industrial operating conditions. Previously, from post reaction *ex situ* XRD and Mössbauer spectroscopy studies,

deactivation of such Au/C catalysts operating above 120 ºC has been attributed to the reduction of gold from its cationic form to generate metallic Au nanoparticles.[16,17] Also the formation of polymeric organic species on the catalyst surfaces, as observed after long reaction periods under industrial conditions, resulting in carbon fibre formation,[7] has been considered as a vector for the deactivation of this class of catalyst. Strategies to inhibit both deactivation pathways include the addition of other metal chlorides or dopants such as nitrogen and phosphorus. [18,19]

The study reported here investigates if the formation of Au(0), which has previously been stated as a deactivation mechanism from post-reaction studies, can be directly correlated with a decrease in VCM productivity under actual reaction conditions. [16,20,21,22,23] In addition, the role of the individual reactants, in particular acetylene, has been studied and correlated with the observed Au speciation, particularly the formation of polymeric organic species on the catalyst surface.[7] In addition, observations of changes in Au L_3-edge XANES spectra during gas switching experiments have been used to further elucidate the reaction mechanism.

RESULTS AND DISCUSSION

Catalyst structure during thermal treatment

Highly active Au/C catalysts prepared by the impregnation of Au from a solution of *aqua regia* have previously been shown to consist of atomically dispersed cationic Au and be highly active for acetylene hydrochlorination.[9] To test the thermal stability of highly dispersed Au species, the catalyst has been heated to 350 °C (at a rate of 5 °C/min) under an inert N_2 atmosphere (to prevent the combustion of the carbon support) while being characterized using *in situ* XRD (Figure 1a). Given that the single site cationic Au species, shown by XANES analysis[9] to be present in catalyst, are undetectable by XRD no diffraction peaks from Au were observed at room temperature. The dispersed Au(III)/Au(I) species in the 1wt % Au/C (1% Au/C-AR) catalyst, showed high thermal stability from ambient temperature up to 250 ºC, with no characteristic reflections of f.c.c. Au being observed over this temperature range. Upon reaching 300 °C, reflections corresponding to the (111), (200), (220) and (310) Au lattice planes became evident demonstrating the formation of discrete Au nanoparticles and implying that the Au species have now become mobile on the support material. Scherrer analysis of the (111) reflection at 300 °C gave an average crystallite size of 29 nm. As expected, the mean nanoparticle size increased even further as the temperature was increased to 350 °C as did the relative intensity of the Au diffraction pattern demonstrating that a greater amount of Au is in a crystalline state.

Clearly 1% Au/C-AR is thermally stable from the perspective of XRD analysis up to 300 °C under an inert atmosphere. However, it should be noted, that even if single-site cationic species are thermally stable under an inert atmosphere, there is significant scope for different $AuCl_x$ species, which are not differentiable by XRD, to exist and evolve during heating. X-ray absorption fine structure (XAFS) can be used to show potential changes in Au oxidation state and speciation. Monitoring the changes in white

line height, a feature detectable in the XANES region which corresponds to the Au $2p_{3/2} \rightarrow 5d$ primary transition (see experimental section for more details), showed that while heating the catalyst to reaction temperature (200 °C) under Ar, the Au(III)/Au(I) ratio significantly changed from Au(III) chloride to Au(I) chloride (Figure 1b).[9] Therefore, while it is true to state single-site cationic species are retained on heating, the speciation and oxidation state changes even in the absence of reactant gases.

XANES analysis of Au/C-AR catalyst under different reactant gases.

It has been postulated, based on combined *in situ* XAFS and DFT studies, that the reaction mechanism for Au catalysed acetylene hydrochlorination proceeds via an oxidative addition and reductive elimination process to generate VCM, which makes the redox properties of the cationic Au species an essential requirement for activity.[7,9] Given the postulated redox mechanism and likely deactivation mechanism, namely the agglomeration and reduction of cationic species to metallic Au, it can be expected that exposure to the reaction mixture or indeed each individual reactant gas has the potential to affect Au speciation. In previous studies, *ex situ* XPS of Au/C catalysts collected after exposure to different combinations of reactants showed that HCl increased the concentrations of Au(III) and Au(I) at the expense of Au(0), while C_2H_2 resulted in a reduction of Au(III) to Au(I).[7] To re-iterate, these experiments were carried out *ex situ*, potentially resulting in significant changes to the Au speciation during removal from the reactor, and exposure to air and moisture before insertion into the XPS instrument. Another important point to note is that relative changes in the concentrations Au(III) and Au(I) species appear minor in comparison to the dominant signal associated with Au(0). A key point to consider in XPS experiments is the significant photo-reduction of gold chloride compounds that can occur, which results in over-estimation of the Au(0) concentration. While appearing counter-intuitive, the higher incident photon energy associated with Au L_3-edge XAFS (11.919 keV for Au L_3-edge XAFS versus 1.487 keV for Al source XPS) results in lower rates of photo-reduction for XAFS experiments compared to Al source XPS, due to the significantly lower absorption cross-section in the former case.[9] For this reason XAFS can be considered a less artefact prone and more representative characterization technique for Au valence state than XPS.

To clarify the influence of both combinations and the individual reactants on Au speciation, under reaction conditions, a sequential flow *in situ* Au L_3-edge XAFS experiment (as detailed in the experimental section) was performed to study the 1% Au/C-AR catalyst. A plot of VCM productivity with respect to reaction time and the normalized white line intensity is shown in Figure 2 during exposure to a well-defined sequence of different reaction gas mixtures. The catalytic behaviour of the 1% Au/C-AR catalyst for the first 240 min under the reaction mixture shows the same trend as in our previous study, in which an induction period of *ca.* 180 min was noted before VCM productivity reached steady state.[9] During this induction period, the normalized Au L_3-edge white line intensity dramatically increased from 0.67 to 0.94 before slowly decreasing back to a value of 0.70 at steady

state. As previously reported,[9] this initial change in white line height is associated with the rapid formation of Au(III) chloride-like species followed by its gradual reduction to one principally containing Au(I)chloride.

After 240 min of reaction the catalyst was then exposed to HCl-only diluted in argon [HCl/Ar] for *ca.* 70 min (*i.e.*, no C_2H_2) at a flow rate matching the total flow of the reaction mixture. As expected, while flowing HCl/Ar only, no vinyl chloride monomer formation was observed. Interestingly, in the XANES region (Figures 2 and 3a) a small decrease in normalized white line height was noted (from 0.70 to 0.68), indicating a very slight reduction in Au oxidation state. The observed value of 0.68 is identical to that of the catalyst at 200 °C in an inert atmosphere. This observation at first sight appears contradictory to the postulate that HCl is the oxidant within the reaction, preventing Au reduction and also facilitating the first step of the reaction mechanism. Indeed, ex situ studies have shown HCl to have oxidised Au(0). However, in the context of oxidising metallic Au the concentration of HCl employed here is significantly lower than in other studies, limiting the oxidation potential of the reaction environment and possibly explaining the lack of Au oxidation in the presence of HCl alone.[7,16,24] Yet this consideration does not explain why a significant increase in normalized white line height is observed under a HCl/C_2H_2 reaction mixture, but not with HCl/Ar alone.

Re-introduction of the full reaction mixture (*i.e.*, $HCl/C_2H_2/Ar$), after HCl/Ar treatment, resulted in an almost immediate return of VCM production (Figure 2), although initially at a marginally lower rate of 2.28 mol $kg_{cat}^{-1}h^{-1}$ compared to the previous steady state productivity rate of 2.74 mol $kg^{-1}\,h^{-1}$. The VCM productivity then steadily increased over the next 115 min before reaching a new steady state productivity value of 2.70 mol $kg_{cat}^{-1}h^{-1}$. During this period of increasing activity, the normalized white line intensity also gradually increased. Clearly, the catalyst was not significantly deactivated under the HCl/Ar atmosphere, although the system was perturbed and a second, albeit smaller, induction period was seen. As the 1%Au/C-AR catalyst was not deactivated by the HCl/Ar gas treatment, but nether underwent oxidation, it is reasonable to conclude that C_2H_2 must somehow assist in the oxidative addition of HCl, facilitating the reaction, based on the Au(I)-Au(III) redox couple. We postulate that C_2H_2 assists in the oxidative addition of HCl in the first step of the reaction mechanism with a concerted HCl and C_2H_2 addition to the Au(I)Cl species. This differs from our previously proposed mechanism,[9] in which the oxidative addiction of HCl to form $AuCl_2H$, was then followed by C_2H_2 addiction and the reductive elimination of VCM. Further supporting evidence for this revised mechanism has been obtained by studying the order of reaction with respect to HCl and C_2H_2 (as discussed later).

Once steady state in step (iii) of the sequence had been reached, the catalyst was exposed to dilute acetylene only [*i.e.*, C_2H_2/Ar] (step iv). In common with the HCl/Ar environment, no VCM production was observed with exposure to acetylene alone. On introduction of C_2H_2/Ar the XANES spectra (Figure

3B) significantly altered, with the gradual loss of features at 11,921 eV (white line) and 11,931 eV, and the simultaneous appearance of a new feature at 11,923 eV along with the absorption edge shifting to higher energy. This new XANES spectra was not clearly attributable to either Au(III) or Au(I) chloride-like speciation. Figure 4 shows a comparison between C_2H_2/Ar XANES spectra and Au(III), Au(I) and Au(0) standards. Therefore, plotting normalized white line values as in Figure 2 was considered to be unsuitable to determine the Au speciation in this instance. Some similarities to the Au(0) standard can be observed for the new feature, although the absorption edge position is noticeably different. While a detailed analysis of this feature is not yet developed, it can be concluded that C_2H_2 strongly influences the observed XANES spectrum through significant changes in electron density at the Au metal centre, as evidenced by the increase in energy of the absorption edge position. Given that exposure of Au catalysts to acetylene without an excess of HCl is known to result in catalyst deactivation,[6] the observed changes in the XANES spectra are evidence of a strong Au-C_2H_2 interaction that is potentially detrimental to the catalytic performance. Further analysis of this species from EXAFS is presented in the following section.

Re-introduction of reactant gases to the 1%Au/C-AR catalyst after C_2H_2/Ar treatment (step (v)) resulted in VCM productivity returning. However, unlike the original induction period (step (i)) or following the HCl/Ar treatment (step (iii)), the productivity did not increase with reaction time. Rather it decreased from 2.24 mol kg^{-1} h^{-1} to 1.79 mol kg^{-1} h^{-1} over 90 min, providing evidence that the Au acetylene interaction occurring in step (iv) had partially poisoned the catalyst. Interestingly, the XANES of the catalyst on re-introduction of HCl/C_2H_2/Ar reactant gases in step (v) show an almost instantaneous return to the more recognisable spectrum with the characteristic a Au(I)/Au(III) features seen in the previous reaction steps (i) through (iii). The re-emergence of an identifiable white line feature could therefore be monitored, whose intensity was found to remain relatively constant ~0.69, with only a marginal increase in height over this final reaction period (Figure 2). Notably, the relationship between normalized white line and VCM productivity has clearly altered relative to that observed initially and after HCl/Ar treatment.

A linear correlation between the normalized white line height and VCM productivity for the initial induction period (step (i) in Figure 2), as previously reported[9] and shown in Figure 5, is strong with a Pearson's correlation coefficient value *r* of -0.994 and observed gradient of 0.104 (±0.002). A similar correlation between normalized white line height and VCM production for the reaction period after HCl treatment (step (iii) in Figure 2) is also evident except that the gradient of the trend line changed to 0.057 (±0.007). A similar plot for the reaction period (step (v)) after C_2H_2 treatment gave a gradient of only 0.009 (±0.005), indicating that the relationship between productivity and normalized white line height was now almost invariant.

The simplest explanation for the loss of correlation after step (v) is that one or more additional spectator species, which contribute to the XANES in the region of the Au(I)/Au(III) white line, are present after treatment with C_2H_2/Ar and to a lesser extent after exposure to HCl/Ar. Such an explanation is supported by comparison of the XANES spectra of the catalyst at steady state for each reaction period (Figure 6); *i.e.,* at the end of the initial induction period (step (i) in Figure 2), at steady state after HCl treatment (step (iii) in Figure 2) and at the very end of the reaction after C_2H_2 (step (v) in Figure 2). A 1eV shift in the position of the white line, between the initial and final steady state spectra, indicates a notable change in Au speciation that is not apparent from white line height measurements alone.

Linear combination fitting (LCF) of these three spectra and those of the catalyst under HCl/Ar and C_2H_2/Ar, using Au(III), Au(I) and Au metal standards, was performed to gain greater understanding of the changes in the XANES spectra and explain the loss in correlation between white line and VCM productivity in step (v) (Table 1). Firstly, fitting of the catalyst under C_2H_2/Ar was not successful, in that no acceptable fit was found with the three standards chosen, further highlighting a strong interaction between C_2H_2 and the gold species present on the catalyst. The catalyst at the end of the first induction period, under HCl/Ar and during the second reaction period were comparable in terms of their Au(III) and Au(I) ratios, however a small amount of metallic Au was possibly to be present of step (ii). Given that the calculated Au(0) concentration was comparable to the estimated error, this result taken in isolation appears of limited value. However, clear evidence of metallic Au (*ca.* 21wt %) was found from LCF of the catalyst after C_2H_2/Ar treatment (step (iv) in Figure 2). As metallic Au is known to be catalytically inactive for acetylene hydrochlorination, this observation correlates well with the loss in activity seen after C_2H_2 treatment. Furthermore, given that Au(0) has a normalized absorption value of 0.6 at the energy of the Au(III) white line (11,920 eV) the presence of this species will reduce the white line intensity in a XANES spectrum of a sample containing Au(III), Au(I) and Au(0). In doing so, the presence of Au(0), will disrupt the correlation between normalized white line height and VCM productivity. An example of how 0, 25 or 50 mol% Au(0) effects the gradient of the white line height versus Au(III):Au(I) is shown in Figure S1 where increasing Au(0) content within the sample decreases the size of gradient of the plot.

Given that LCF, using reference $KAuCl_4$, $[AuCl_2]^-$ and Au foil materials, cannot comprehensively model single-site $AuCl_x$ species supported on a carbon surface, previous studies used the simpler analysis of white line height to give an average Au oxidation state. While white line height was satisfactory for analysis of the initial analysis (induction period and initial steady state testing) of a 2 component system (Au(I) chloride and Au(III) chloride), LCF despite its flaws becomes required in this more complex multi-speciation system.

EXAFS analysis of Au/C-AR catalyst under different reactant gases.

While XANES analysis provides relevant information concerning Au speciation, the complex nature of the spectra requires additional EXAFS analysis to clarify interpretation. EXAFS of the catalyst at steady state reactivity, before and after HCl/Ar treatment, and after C_2H_2 treatment, can provide further evidence of an increased contribution from metallic Au after sequential gas treatments. Figure 7 shows the magnitude of the Fourier transform data of the catalyst at the end of steps (i), (iii) and (v) in the reaction profile. The predominant feature in all samples is that of 1st shell Au-Cl interactions with multiple Au-Cl scattering events beyond 3 Å. However, features associated with Au-Au interactions between 2.5 and 3 Å also become noticeable after treatment with C_2H_2 (although the FT magnitude is small) confirming the deduction form linear combination fitting of the XANES that metallic Au nanoparticles are generated during exposure to C_2H_2/Ar.

EXAFS analysis (Figures S2 and S3, Table 2) can also provide further information on the nature of the Au speciation, especially while the catalyst was under an C_2H_2/Ar only environment. While the Au L_3 edge XANES of this species was clearly different to Au (I) or Au(III)chloride, EXAFS shows that Au-Cl interactions are still present in the C_2H_2/Ar treated sample. The magnitude of this scattering in the Fourier transform data (Figure S3) is significantly lower under C_2H_2/Ar than the catalyst in the presence of both reactants (C_2H_2 + HCl/Ar). No additional features associated with Au-C or Au-Au interactions were observed in the C_2H_2 treated material suggesting no significant Au-C_2H_2 complex or Au(0) nanoparticle formation. Taking this into account, along with the dampened oscillations at higher wavenumbers in the χ-space data (Figure S2), a model of $AuCl_x$ with two Au-Cl bond lengths that were partially out of phase was considered. The results of fitting two 1st shell Au-Cl lengths to the data are given in Table 2 which yields an Au-Cl combined coordination number of 1.8(4) compared to that of 2.5(1) for the catalyst under normal steady state conditions (fitted with a single Au-Cl distance). It should be noted that no reasonable fitting of 2 Au-Cl paths was obtainable for any other sample investigated in steps (ii), (iii) and (v). It was observed that a small component of the Au-Cl interactions in the catalyst under C_2H_2/Ar were notably shorter, at 2.110(57) Å compared to the 2.273(6) Å for the catalyst at steady state conditions. Therefore, we conclude that the presence of excess acetylene results in the formation of some shortened Au-Cl interactions, but with no direct evidence of Au-C_2H_2 bond formation. It should also be noted that evidence of multiple Au-Cl distances was also previously observed during the induction period of the Au/C-AR catalyst in step (i) and illustrates that complex interactions between $AuCl_x$ are present even under standard reaction conditions.[9]

EXAFS analysis (Table 2) of the catalyst at steady state under HCl/Ar (step (ii)) and the second reaction mixture HCl/C_2H_2/Ar (step (iii)) showed little difference to that at steady state in the first reaction period. A slight reduction in Au-Cl CN number under HCl/Ar was observed, in-line with the moderate reduction in white line height also noted during this period. For the sample at steady state after the C_2H_2/Ar cycle, (*i,e.*, at the end of step v)), a model with both a Au-Cl and a Au-Au interaction was

found to provide good fitting parameters, further supporting the presence of metal in the deactivated catalyst.

XAFS sequential flow experiments highlighted several interesting observations that have not been observed in previous *ex situ* studies; namely (i) the oxidation of the Au(I)-Cl species appears far more facile in the presence of C_2H_2 and (ii) that C_2H_2 directly interacts with $AuCl_x$ species significantly altering the XANES spectra and changes Au-Cl lengths when no HCl is present. The first point regarding Au(I)-Cl oxidation can be further clarified by performing kinetic studies of the reaction to determine orders of reaction with respect to the reactant gases. If the apparent requirement for Au(I)-Cl oxidation is the concerted addition of HCl and C_2H_2 (as suggested from XANES data), and if this step is rate limiting, then the reaction should be first order dependent with respect to each reactant. To prevent apparent zero order responses, each reactant investigated was studied over a range of highly dilute concentrations. The linear dependence of both HCl and C_2H_2 reaction rate, as shown in Figure 8, demonstrates 1st order dependence with respect to each reactant and 2nd order reaction kinetics overall. The combined evidence from in-situ XANES experiments and the measured 1st order dependence for each reactant provides strong evidence for a concerted HCl and C_2H_2 addition to the Au(I)-Cl active site.

Inelastic Neutron Scattering (INS): the effect of C_2H_2 on Au complex speciation

Vibrational spectroscopy provides a viable method to clarify the effect of C_2H_2 on Au complex speciation, as seen during the C_2H_2/Ar treatment in step (iv) of the reaction sequence. As the carbon support in the catalyst would be highly absorbent of infra-red radiation, we attempted inelastic neutron scattering (INS) spectroscopy. While INS is suited to observing hydrogen speciation in the C_2H_2/Ar treated sample and therefore the nature of the Au complex, it suffers from low signal-to-noise (due to the required interaction of the neutron with the small nucleus of the absorber). To mitigate this problem a more heavily loaded 2wt % Au/C-AR sample was prepared to increase the concentration of Au species available for interaction with acetylene in the sample. XAFS, XRD and STEM analysis of the 2wt % Au/C-AR material demonstrated that this more highly loaded catalyst still comprised of single site cationic Au species with a negligible concentration of metallic gold nanoparticles (Figure S4, Figure 9a-d).

The 2wt % Au/C-AR catalyst was sequentially treated under helium, a dilute acetylene gas mixture (5%C_2H_2/He or concentrated acetylene (100%) in a reaction cell for *ca.* 30 minutes at 200 ˚C. Between each step the sample was cooled (to minimise Debye-Waller contributions), and the cell flushed with He prior to acquisition of the INS spectrum. The resulting spectrum provides detail of acetylene species while the catalyst is exposed to an excess of acetylene under reaction conditions. The spectra of 2wt % Au/C-AR sample prior to acetylene treatment (used as a background spectrum), 2wt % Au/C-AR after

treatment in 5% acetylene and 100% acetylene are shown in Figure S5. Reaction with the C_2H_2(5%)/He mixture resulted in no observable changes in the spectrum, whereas in contrast reaction with 100% C_2H_2 results in bands at 2990, 1295, 961, 700 and 640 (and possibly 400) cm^{-1}. The difference spectra: (C_2H_2 (5%) dosed minus the background), (C_2H_2 100% dosed minus the background), (C_2H_2 (100%) dosed minus C_2H_2 (5%) dosed) are shown in Figure 10.

INS spectra of metal-acetylide, silver,[25,26] silver/copper,[27] copper,[28,29] and gold,[30,31,32,33,34] complexes have been widely reported. The bands seen in the difference spectra of (100%) C_2H_2 -background were compared to that of Au–C≡C–H modelled as: an isolated molecule, an adsorbed molecule on a single carbon atom of a graphene sheet (to model the carbon support) and an adsorbed molecule above the centre of a graphene hexagon (see Figure S6). All three models exhibit ≡C–H stretches at ~3300 cm^{-1}, a C≡C stretch at ~2000 cm^{-1}, a C≡C–H bending mode at ~600 cm^{-1} and an Au–C stretch at ~250 cm^{-1}. As shown in Figure 11, none of the calculated spectra match the observed spectrum of the catalyst after acetylene treatment. Given the possibility of Au(0) formation after acetylene treatment as suggested from LCF of XANES and EXAFS analysis, models for acetylene bound to Au nanoparticles were also considered. However, in common to the metal-acetylide spectra no correlation could be found between the models of acetylene bound to an Au_4 tetrahedron (representing a small Au cluster) and the experimental spectrum.

An alternative assignment to the observed bands on the 2wt % Au/C-AR catalyst after C_2H_2 treatment is that of oligomerised acetylene species. Previously, carbon fibres have been observed by TEM analysis to have grown on spent Au/C-AR catalysts after 24 daystime-on-line.[6] The INS spectrum of polyacetylene shown in Figure 12 exhibits bands at similar energies to those seen on the 2wt % Au/C-AR catalyst after C_2H_2 treatment.[35] However, there are several modes absent in the 2wt % Au/C-AR catalyst after C_2H_2 treatment, as compared to polyacetylene. Potentially these absent modes are associated with shorter oligomeric species on the catalyst surface. To test this possibility, *all-trans*-1,3,5,7-octatetraene (inset in Figure 12) was used as a model for a short chain acetylene oligomer. Figure 12 compares the experimental and calculated spectra and indicates good agreement, particularly regarding the 1295 cm^{-1} mode that is clearly present.

The used catalyst after the INS experiment was then analysed *ex situ* by XAFS and STEM (Figure S7). The XANES spectrum recorded is almost identical the one obtained for the 1% Au/C-AR catalyst during the step (iv) of the sequential flow experiment (C_2H_2/Ar). Moreover also in this case, the Au-Cl intensity in the EXAFS is decreased compared to the spectrum of the freshly prepared catalyst showed in Figure S7 while the STEM-HAADF images (Figure 13) show that the gold is still pre-dominantly dispersed as atomic on the carbon support

The INS data shows for the first time the presence of oligomeric acetylene species, while the Au XANES shows a clearly altered Au species after C_2H_2 treatment. Unfortunately, there is no clear evidence that these two species are connected, as no evidence of Au-acetylene bonding was found from either XANES or INS. However, we provide clear evidence of the significant surface acetylene species that become evident on exposure to a C_2H_2 excess in a reactant gas mixture, which is known to be detrimental to catalytic activity.

***In situ* deactivation of 2% Au/C-AR during the acetylene hydrochlorination reaction**.

Catalyst deactivation, associated with Au(0) formation and a loss of the correlation between white line height and VCM productivity was observed in the 1% Au/C-AR catalyst over multiple different sequential gas experiments. To clarify if a similar deactivation process occurs, without various sequential gas treatments, a continuous extended time-on-line experiment with a constant gas composition coupled with *in situ* XAFS monitoring could in principle be performed. Such an experiment is not easily carried out with a 1wt % Au/C-AR catalyst as the deactivation period is too long to be monitored over a single synchrotron beam time experiment. However, the 2wt % Au/C-AR catalyst used for INS studies, with its comparable initial single-site dispersion of $AuCl_x$ species, would be expected to undergo a more rapid deactivation associated with Au(0) particle formation, due to the higher concentration of Au available for agglomeration.

The structural behaviour of the 2wt % Au/C-AR catalyst was found to be initially comparable with that of the 1wt% Au/C-AR material, with a decrease in normalized white line height upon heating under Ar, from 1.07 at 25 °C to 0.68 at 200 °C (Figure S8). Linear combination fitting of the 2wt % Au/C-AR catalyst at 200 °C confirmed the absence of Au(0), before introduction of the reaction mixture. As the reaction mixture was introduced the normalized white line increased from 0.68 to 0.85 (Figure 14a), as observed in the 1wt% Au/C-AR catalyst. The white line height then began to decrease over a 20 min period, commensurate with an increase in VCM productivity, as seen for the induction period of the 1wt % catalyst. From this point in the reaction the evolution of VCM productivity and association with normalized white line height, diverges for the 2wt % Au/C-AR catalyst. After *ca*. 40 min reaction, the higher loading catalyst undergoes a gradual and prolonged loss in activity, with VCM productivity dropping by 40% between 40 and 200 min time-on-line. As predicted from the sequential gas experiments, on the 1wt % Au/C-AR catalyst, the observed normalized white line height remained relatively consistent over the deactivation period. As the reaction proceeded for another 150 min, EXAFS and LCF showed that the catalyst developed considerable amounts of metallic Au (*ca*. 22.5 %), in addition to $AuCl_x$ species (Figures 14a and 14b and Figure 15).

HAADF-STEM images of the used 2wt % Au/C-AR catalyst confirmed the presence of single-site species in addition to larger particles of Au (Figures 16a-c) in the 20-100 nm size range. This

observation suggests that once the $AuCl_x$ single site species reduced to Au(0), sintering occurred very efficiently under reaction conditions. Counting the numbers of Au atoms over certain areas of the carbon support from several HAADF-STEM images gave estimated Au atom densities of 0.470 atoms/nm^2 and 0.154 atoms/nm^2 for the unused and used 2wt % Au/C-AR catalysts respectively (see Table 3). This suggests that ~2/3 of atomic Au transformed into large Au particles during the reaction, leading to a significantly decreased Au dispersion.

CONCLUSIONS

Single site Au/C catalysts, prepared by impregnation and using *aqua regia* Au solution, were studied by XAFS and INS under various reactant gas compositions to gain a greater understanding of the reaction mechanism and mode of catalyst deactivation. Sequential gas experiments showed that HCl, in the absence of C_2H_2 cannot re-oxidise Au(I)-chloride species under the reaction conditions studied, and that HCl addition requires concerted addition with C_2H_2. Exposure of the Au/C catalyst to C_2H_2 (in the absence of HCl) resulted in a XANES spectrum that did not resemble Au(III) chloride, Au(I) chloride or Au(0), while EXAFS analysis suggested that $AuCl_x$ species were retained, but with distorted Au-Cl distances. INS studies of a Au/C catalyst exposed to C_2H_2 showed that oligomeric acetylene species formed on the catalyst surface, which could act as potential precursors to carbon fibre formation and thus become a significant deactivation process.

Catalyst deactivation, after C_2H_2 treatment or prolonged time-on-line studies with higher Au loadings, was found to be associated with the formation of metallic Au particles. The presence of Au(0) significantly affected the strong correlation between normalized white line height and VCM productivity seen in a completely single-site catalyst (*i.e.*, in the absence of Au(0) particles). Care must be taken to consider other spectator species that may be present from catalyst preparation or evolve during the reaction. Simple descriptors of catalyst structure, such as white line height, while useful, must be carefully used in systems of increased complexity.

Supporting Information

Effect of the Au(0) contribution in the correlation between white line height and Au(III)/Au(I) ratio, further EXAFS data of the 1wt %Au/C-AR catalyst during the sequential gas experiment, XRD/XAFS/STEM/INS characterization of the freshly prepared and used 2wt % Au/C-AR catalyst, proposed models for INS data spectra simulations.

Acknowledgements

The authors wish to thank Cardiff University for support as part of the MAXNET Energy Consortium. UK Catalysis Hub is thanked for resources and support provided through our membership of the UK Catalysis Hub Consortium and funded by the Engineering and Physical Sciences Research Council (EPSRC) (grants EP/K014706/1, EP/K014668/1, EP/K014854/ 1EP/K014714/1, and EP/M013219/1). We used the B18 beamline at the Diamond Light Source (allocation numbers SP10306, SP11398, and SP15214) with the help of D. Gianolio and G. Cibin. We gratefully acknowledge the Science and Technology Facilities Council (STFC) for access to neutron beamtime at ISIS, and also for the provision of sample preparation, Merlin facilities. C.J.K. acknowledges funding from the National Science Foundation Major Research Instrumentation program (GR no. MRI/DMR-1040229). We thank Johnson Matthey for their contribution to and funding of this work. We thank S. Morris for technical support.

EXPERIMENTAL SECTION

Catalyst preparation. 1 and 2wt % gold supported on activated carbon catalysts were prepared by wet impregnation of the $HAuCl_4$ precursor dissolved in *aqua regia* (denoted respectively as 1wt % Au/C-AR and 2wt % Au/C-AR materials). Activated carbon (Norit ROX 0.8) was initially ground to obtain a 100 - 140 mesh powder. The gold precursor, $HAuCl_4 \cdot xH_2O$ (Alfa Aesar, 99.9% (metals basis), Au 49%) was dissolved in *aqua regia* (3 parts by volume HCl [(Fisher, 32wt %)]: 1 part by volume HNO_3 [(Fisher, 70wt %)]). The gold precursor solution was then added drop-wise with stirring to the activated carbon. Stirring was continued at ambient temperature until NO_x production had subsided. The product was then dried for 16 h at 140 ºC under an inert flow of nitrogen.

In-situ powder X-ray Diffraction (XRD). Powder XRD data were acquired using an X'Pert Pro PAN Analytical powder diffractometer employing a Cu K_α radiation source operating at 40 keV and 40 mA. Analyses of the spectra were carried out using X'Pert High Score Plus software. The mean crystallite size of the metallic gold nanoparticles was determined using the Scherrer equation assuming a spherical particle shape and a K factor of 0.9 on the reflection arising from the {111} Au planes (at $2\theta = 38°$).

In-situ X-ray absorption fine structure (XAFS). XAFS spectra were recorded in transmission mode at the Au L_3 absorption edge, at the B18 beamline of the Diamond Light Source, at Harwell, UK. The

measurements were performed using a QEXAFS set-up with a fast-scanning Si (111) double crystal monochromator. For the *in situ* measurements, the time resolution of the data acquisition was 20s per spectrum.

X-ray absorption near-edge structure (XANES) analysis was mainly focused on understanding the details of the white line feature detectable at an absorption energy of ~11920 eV which corresponds to the Au $2p_{3/2} \rightarrow 5d$ primary transition. Three different Au standards were used to perform a linear combination fitting (LCF) analysis of the Au L_3-edge XANES: namely $KAuCl_4$/$[AuCl_4]^-$ for Au(III), $[AuCl_2]^-$ for Au(I) , and a bulk Au-foil for Au(0). The normalized white line intensity values observed for the $[AuCl_4]^-$ and $[AuCl_2]^-$ standards were 1.1 and 0.6, respectively.

Analysis of the extended X-ray absorption fine structure (EXAFS) data was performed using IFEFFIT with the Demeter software package (Athena and Artemis).[36,37] 1st shell Au paths were fitted at all k weighted χ data, using a k space window of 3-11 and an R window of 1.25-2.60. The Debye-Waller ($2\sigma^2$) and the amplitude reduction (S_o^2) factors were fixed during fitting of data at 0.0037 $Å^2$ and 0.75 respectively. These values were determined from fitting of $KAuCl_4$ at a known temperature and with a fixed coordination number (CN) of 4.[9]

Inelastic Neutron Scattering (INS). For INS analysis, the required amount of 2% Au/C-AR catalyst was loaded into a Conflat sealed stainless steel cell and then dried at 200 °C under vacuum. INS spectra of the dried catalyst were recorded with the MERLIN spectrometer at the ISIS Facility,[38] using incident energies of 600, 250 and 100 meV to observe the C–H/O–H stretch, in-plane C–C stretches/C–H bends and the out-of-plane deformations respectively. These spectra were used as backgrounds for all subsequent spectra. The catalyst was then dosed with C_2H_2(5%)/He at 200 °C. After measurement of the spectra, the catalyst was then dosed with 100% C_2H_2 at 200 ºC and the spectra measured. All the spectra were recorded at <20 K to minimise the Debye-Waller factor.

Computational studies of model systems were carried out using the plane-wave pseudo-potential code CASTEP. Isolated molecule calculations were carried out with the molecule in the centre of either a 10 × 10 × 10 Å or a 15 × 15 × 15 Å box. To investigate the effect of the surface, the same molecules were placed above a single graphene layer with a 10 Å vacuum gap. The Perdew-Burke-Ernzerhof (PBE) functional was used, the plane-wave cut-off was 750 – 1000 eV. For the isolated molecules only the Γ-point was included, for the surface calculations a Monkhorst-Pack grid of 8 × 8 × 1 (12 k-points) or 9 × 9 × 1 (20 k-points) was used. The calculations were converged to better than ± 0.003 eV $Å^{-1}$. After geometry optimisation, the vibrational modes were calculated using density functional perturbation theory as implemented in CASTEP.[39] The CASTEP output includes the vibrational transition energies

and the atomic displacements of the atoms in each mode. The latter enables visualisation of the modes using Materials Studio and is also the input to the program AbINS,[40] that creates simulated INS spectra. AbINS can generate the full 2D $S(Q,\omega)$ map for comparison with the output of direct geometry INS spectrometers such as MERLIN. Cuts through the data assume constant resolution and have the correct Q-dependence and treatment of the Debye-Waller factor so that comparison with experimental data is both straightforward and reliable.

Scanning Transmission Electron Microscopy (STEM). Materials for examination by STEM were dry dispersed onto a holey carbon TEM grid. These supported fragments were examined using BF- and HAADF-STEM imaging mode in an aberration corrected JEOL ARM-200CF scanning transmission electron microscope operating at 200kV. This microscope was also equipped with a Centurio silicon drift detector (SDD) system for X-ray energy dispersive spectroscopy (XEDS) analysis.

Catalytic testing experiments: activity and deactivation measurements. The 1wt % and the 2wt % Au/C-AR catalysts were tested using a completely automated reactor system with the same set-up as previously described. [8] All the pre-dilute gases 5% C_2H_2/Ar (BOC), 5% HCl/Ar BOC) and Ar (99.99 % BIP, Air Products) were dried using moisture traps before being introduced into the reactor. In all cases, the reactor was heated to 200 °C at a ramp rate of 5 °C/min and held at temperature for 30 min under a flow of argon prior to admitting the hydrochlorination reaction mixture. The tests were performed by using a fixed-bed polyimide (Kapton) microreactor containing the catalysts, keeping the total flow of 50 mL min^{-1} and a total gas hourly space velocity (GHSV) of ~14,000 h^{-1}. When both reactants were present, the C_2H_2: HCl ratio was kept at a constant value of 1:1.02.

The sequential flow experiment (reaction sequence 1) was performed using the 1% Au/C-AR catalyst while simultaneously monitoring the Au L_3-edge XAFS and catalytic activity.

Reaction sequence (1) employed the following gas compositions; step (i) = HCl/C_2H_2/Ar; step (ii) = HCl/Ar; step (iii) = HCl/C_2H_2/Ar; step (iv) = C_2H_2/Ar and step (v) = HCl/C_2H_2/Ar.

The duration of each step in the sequence was not the same. The gas composition during the experiment was altered only when no further change in the XAFS spectra was observed. For this reason, the duration of each step in the reaction sequence was as follows: step (i) = 240 min; step (ii) = 75 min; step (iii) = 120 min; step (iv) = 70 min and step (v) = 90 min.

The reaction mixture was analysed on-line by mass spectrometry (Hiden QGA) and Professional Edition software was used for both qualitative and quantitative analyses. The catalyst activity presented

is shown in terms of productivity towards vinyl chloride monomer (VCM). The response factor of the mass spectrometer towards VCM was correlated with the productivity (mol kg_{cat}^{-1} h^{-1}) obtained by using a Varian 450 gas chromatograph equipped with a flame ionisation detector (FID). Chromatographic separation and identification of the products was carried out using a Porapak N packed column (6 ft × 1/8″ stainless steel). Using the correlation obtained between productivity and VCM mass spectrometer response, it was possible to deduce the productivity for the catalytic reactions performed.

Determination of orders of reaction with respect to the reactant gases. The reactions were performed using the same reactor set-up as described above. The reaction mixture, before and after reaction was analysed by gas chromatography. The results are presented in terms of acetylene conversion (%). The following reaction conditions were employed: Mass of catalyst: 0.045 g; Temperature: 200 °C; Total flow of gases: 50 mL/min; Gas make-up: 5% C_2H_2/Ar, 5% HCl/Ar, Ar; Initial gas concentrations: 2.30% C_2H_2/Ar, 2.35% HCl/Ar. The concentration of C_2H_2/Ar was then altered (from % C_2H_2/Ar = 0.23 – 0.29 – 0.35 – 0.41 – 0.47) maintaining constant the concentration of HCl/Ar or the concentration of HCl/Ar was changed (% HCl/Ar = 0.90 - 1.60 - 2.35 - 3.10) maintaining a constant concentration of acetylene/Ar.

Table 1. Linear combination fitting of the 1wt % Au/C-AR catalyst at the end of each sequence of gas switching. Percentage Au associated with Au(I) chloride (standard $[AuCl_2]^-$); Au(III) chloride (standard $KAuCl_4$) and Au (0) metal (standard Au foil).

Reaction sequence; step (i) = $HCl/C_2H_2/Ar$; step (ii) = HCl/Ar; step (iii) = $HCl/C_2H_2/Ar$; step (iv) = C_2H_2/Ar and step (v) = $HCl/C_2H_2/Ar$.

Reaction step[1]	**Quantification (%)**		
	Au(III)	**Au(I)**	**Au(0)**
1st Reaction mixture (step (i))	28(4)	71(3)	0(3)
HCl/Ar (step (ii))	25(5)	75(3)	0(4)
2nd Reaction mixture (step (iii))	24(5)	72(3)	4(4)
3nd Reaction mixture (step (iv))	20(3)	63(2)	21(2)

NB. Analysis of step (iv) (C_2H_2/Ar) is excluded due to a poor fit.

Table 2. ***In situ*** **EXAFS fitting for Au L_3-edge data of the 1wt % Au/C-AR catalyst during the sequential gas experiment.**

Reaction step[1]	Scattering path[2]	Coordination number	R (Å)	E_f (eV)	R factor
1st Reaction mixture (step i)	Au-Cl	2.5(1)	2.27(1)	1.2(9)	0.0012
HCl/Ar (step ii)	Au-Cl	2.4(1)	2.27(1)	3.3(0.99)	0.007
2nd Reaction mixture (step iii)	Au-Cl	2.5(1)	2.27(1)	2.55(66)	0.004
C_2H_2/Ar (step iv)	Au-Cl (1)	1.4(2)	2.29(3)	1.04(2.84)	0.026
	Au-Cl (2)	0.5(2)	2.11(6)		
3nd Reaction mixture (step v)	Au-Cl	1.7(3)	2.26(1)	2.24(1.89)	0.013
	Au-Au	1[4]	2.84(5)		

Fixed Parameters[3]: $S_o^2 = 0.75$ and $2\sigma^2$ (Å^2) = 0.0037

1) EXAFS data was taken under steady state conditions during each sequential gas sequence step (*i.e.*, when no change in three consecutive spectra was observed).
2) Fitting with multiple Au-Cl paths was attempted for all spectra. However, apart from C_2H_2/Ar (step iv), unrealistic fits such as high R factors and/or negative amplitudes for second paths were obtained.
3) Debye-Waller and amplitude reduction factors were calculated from the fitting of a $KAuCl_4$ standard with a fixed CN of 4.
4) Fittings of the Au-Cl and Au-Au for step (v) were performed fixing the Au-Au coordination number to 1.

Table 3. Atom density measurements from sets of STEM images of the 2wt % Au/C-AR catalyst before and after acetylene hydrochlorination reaction.

2wt % Au/C-AR fresh				2wt % Au/C-AR post reaction			
Image	**Atoms counted**	**Area (nm^2)**	**Area density (atoms nm^{-2})**	**Image**	**Atoms counted**	**Area (nm^2)**	**Area density (atoms nm^{-2})**
1	146	338.26	0.432	**7**	84	247.46	0.339
2	105	314.24	0.334	**8**	102	821.91	0.124
3	130	378.42	0.344	**9**	52	312.86	0.166
4	41	142.54	0.288	**10**	28	348.76	0.080
5	104	94.60	1.099	**11**	46	294.32	0.156
6	193	262.80	0.734				
Total	719	1530.86	0.470	**Total**	312	2025.32	0.154

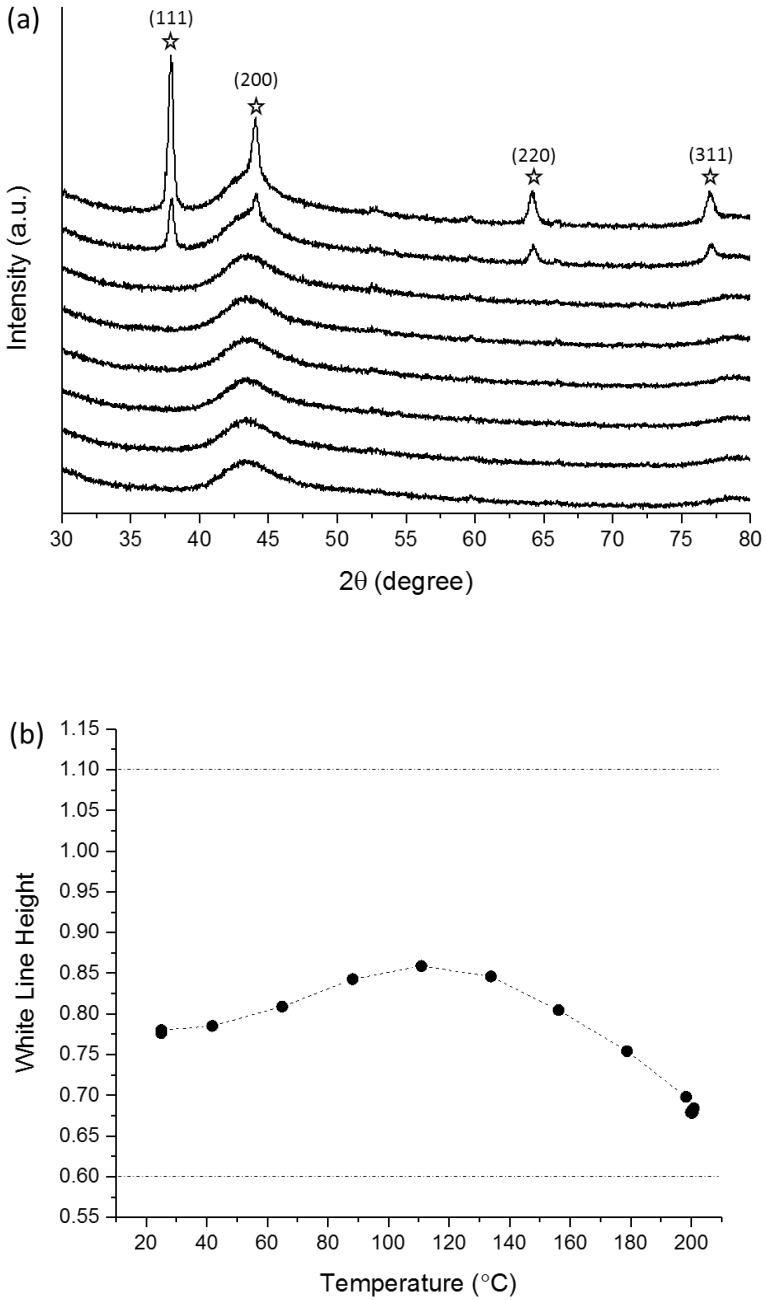

Figure 1. *In situ* characterization of the 1% Au/C-AR. (a) Powder X-ray diffraction (pXRD) patterns acquired at increasing temperatures under inert nitrogen atmosphere. **(b)** Changes in white line height during heating to reaction temperature (200 °C) under Ar at 5 °C min^{-1} (Dotted lines represent the white line intensities of the Au(I) $[AuCl_2]^-$ standard (value of 0.6) and the Au(III) $KAuCl_4$ standard (value of 1.1)).

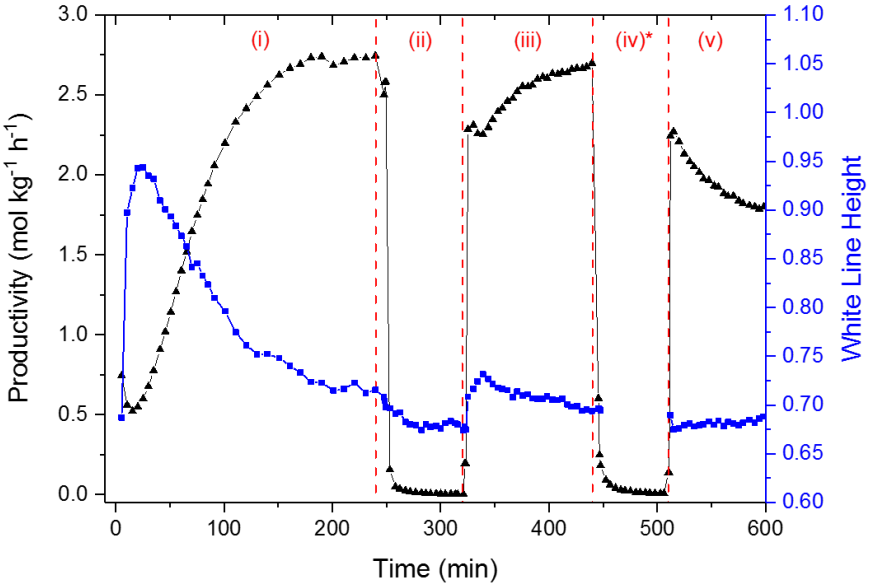

Figure 2. VCM productivity during the sequential gas exposure experiment combined with *in situ* Au L_3-edge XANES data of 1wt % Au/C-AR. VCM production (black triangles) as a function of time-on-line during the sequential gas experiment and the corresponding normalized white line intensity values (blue squares) derived from XANES measurements. Where: (i) HCl+C_2H_2/Ar, (ii) HCl/Ar, (iii) 2nd HCl+C_2H_2/Ar, (iv) C_2H_2/Ar and (v) 3rd HCl+C_2H_2/Ar exposure. (*: no white line data is shown for step (iv) in the sequence).

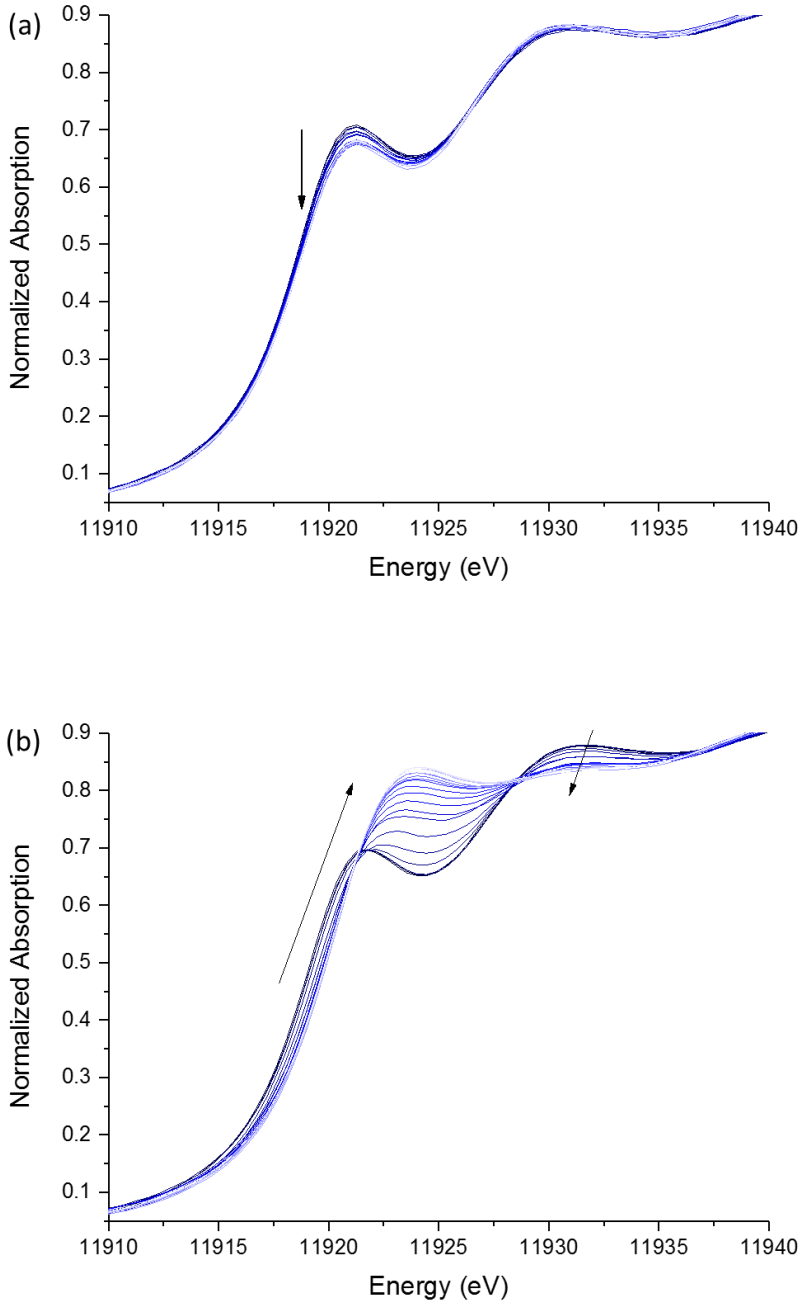

Figure 3. Evolution of XANES spectra during (a) step (ii) (HCl/Ar) and (b) step (iv) (C_2H_2/Ar).

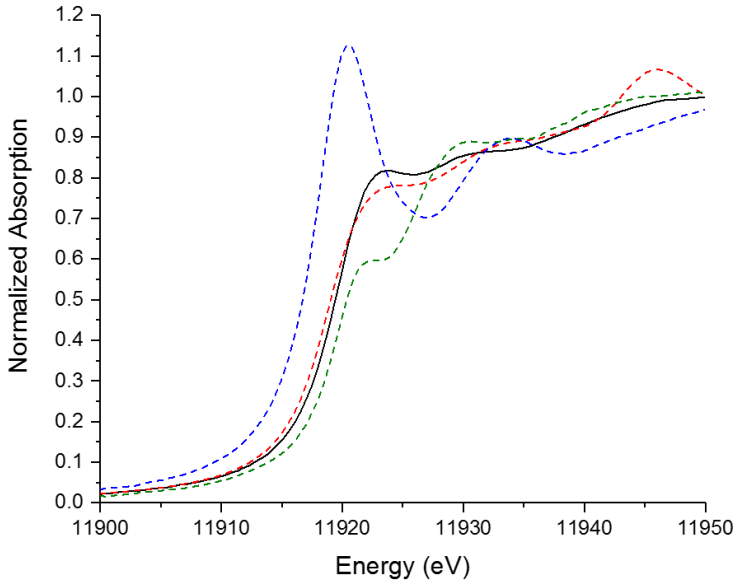

Figure 4. Comparison of Au L_3-edge XANES of the 1wt % Au/C-AR catalyst under an C_2H_2/Ar atmosphere to Au(III) chloride, Au(I) chloride and a metal standard. *Black solid line*; 1wt % Au/C-AR catalysts under C_2H_2/Ar, *blue dashed line*; Au (III) standard of $KAuCl_4$, *green dashed line*; Au(I) standard of $[AuCl_2]^-$, and *red dashed line*; Au (0) metal foil.

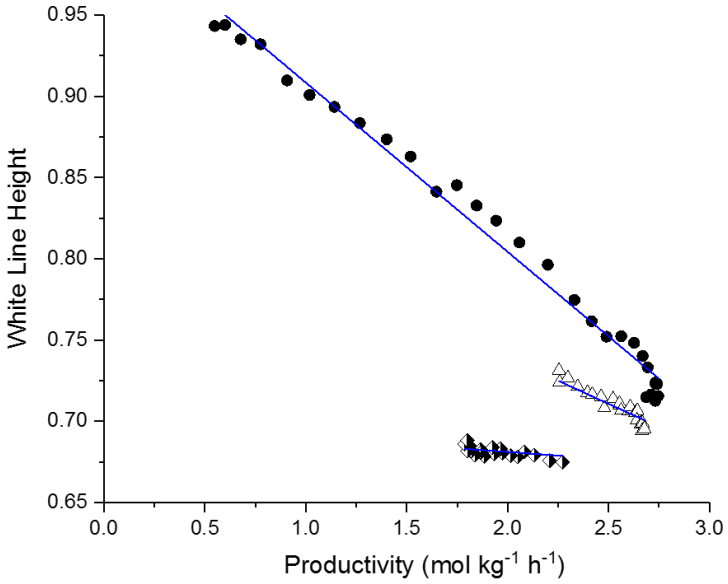

Figure 5. Comparison of white line height versus VCM productivity for the 1wt % Au/C-AR catalyst under HCl/C_2H_2/Ar reaction gas after different single reactant gas treatments. *Solid black circles*; catalyst during first induction period (productivity and white line data from step (i), Figure 2), *open triangles*; catalyst after HCl/Ar treatment (productivity and white line data from step (iii), Figure 2) and *half-filled diamonds*; catalyst after C_2H_2/Ar treatment (productivity and white line data from step (v), Figure 2).

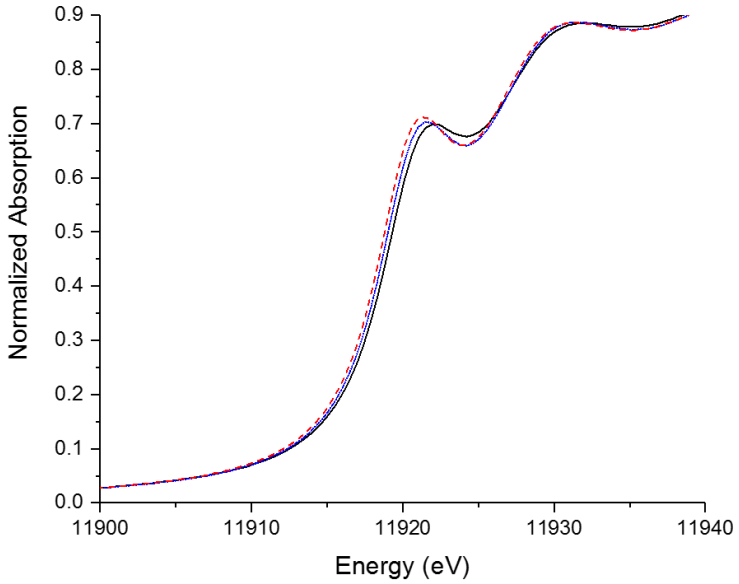

Figure 6. XANES spectra of the 1wt % Au/C-AR catalyst at steady acetylene hydrochlorination conditions after different sequential gas treatments. *Red dotted line*; 1st reaction (step (i), Figure 2), *blue dotted line*; 2nd reaction (step (iii), Figure 2 - after HCl/Ar treatment) and *black solid line;* 3rd (step (v) Figure 2- after C_2H_2 /Ar treatment).

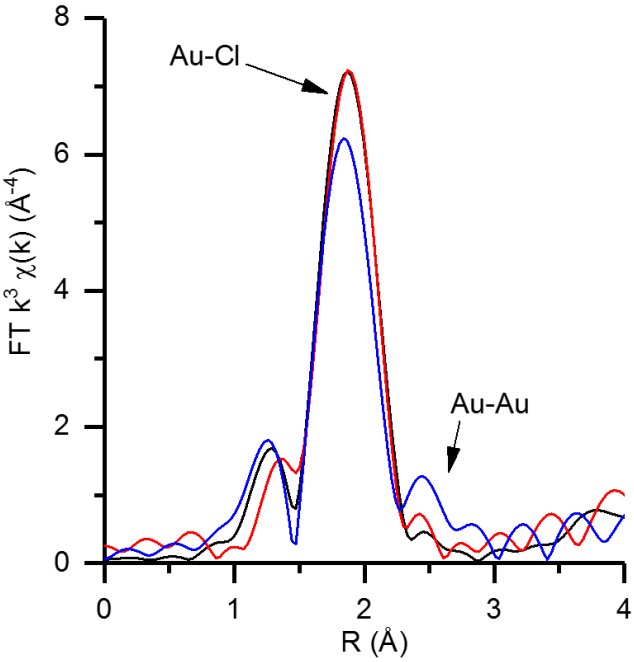

Figure 7. Magnitude of Fourier Transform (FT) of extended X-ray absorption spectra k^3 weighted of 1wt % Au/C-AR catalyst under steady state reaction conditions. *Black line*; FT of catalyst in step (i), *red line*; FT of catalyst in step (iii), *blue line*; FT of catalyst in step (v).

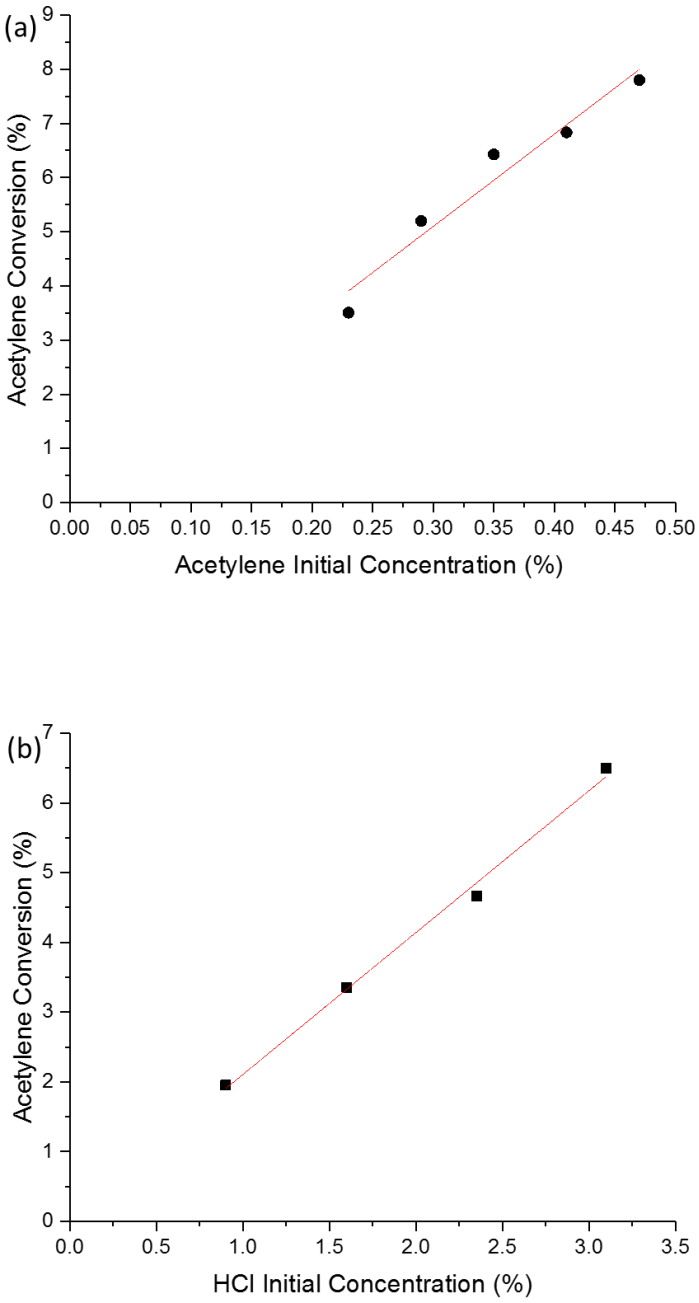

Figure 8. Determination of orders of reaction with respect to the component reactant gases. A linear dependence was found for both (a) C_2H_2 concentration and (b) HCl concentration on reaction rate. *Reaction conditions*: Catalyst (0.045 g), 200 °C, ambient pressure, various concentrations of gases (HCl in excess) balanced with Ar at a fixed flow of 50 mL min^{-1}.

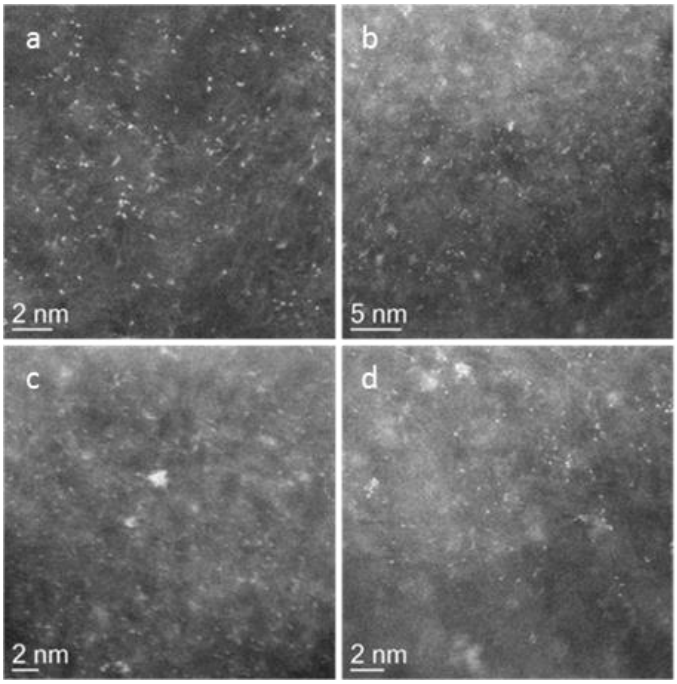

Figure 9. HAADF-STEM images of the 2wt % Au/C-AR catalyst before use. In the unused sample atomically dispersed Au could be easily seen **(a,b)**, while a small number of sub-nm Au clusters were also present **(c,d)**.

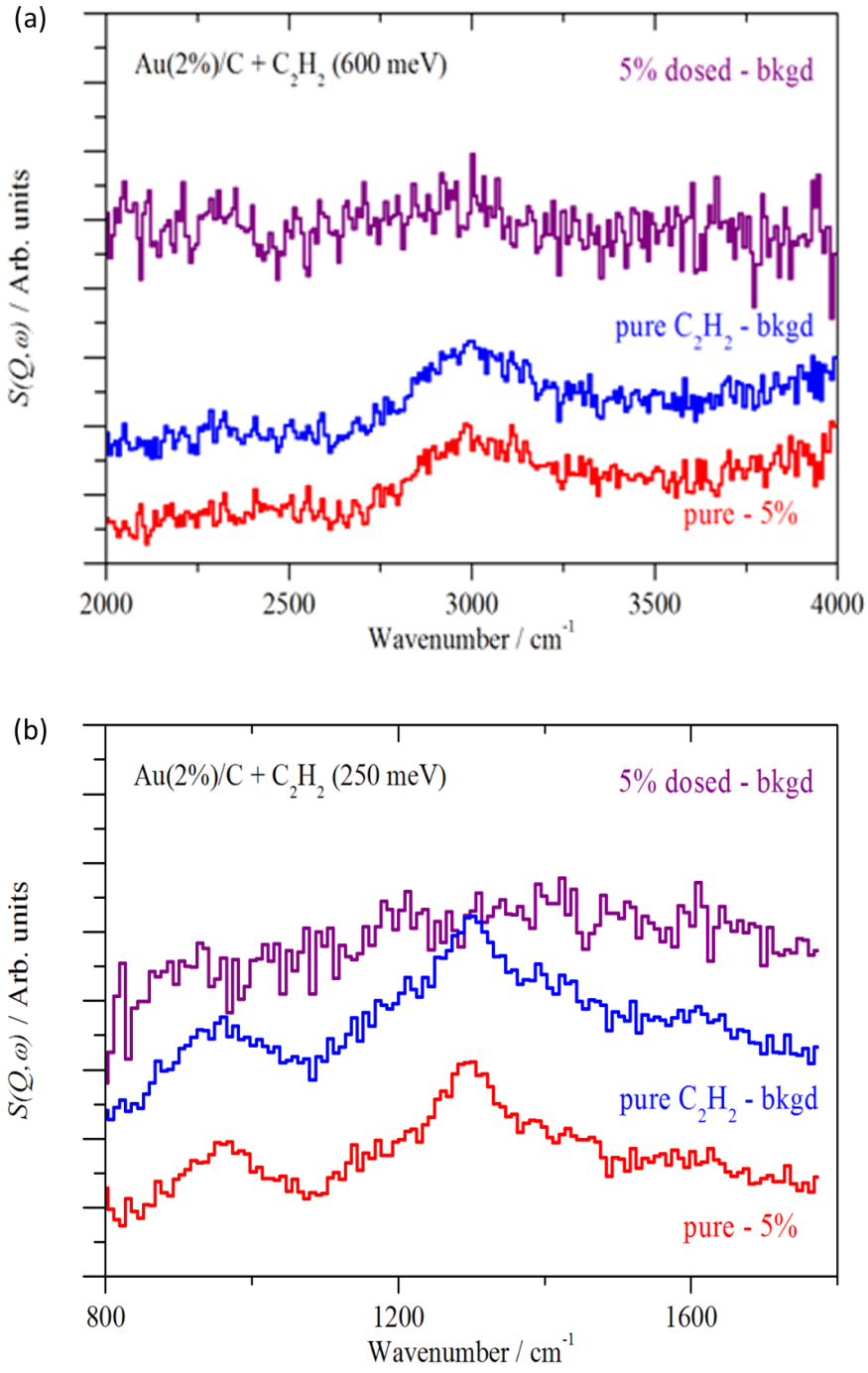
(a)
Au(2%)/C + C2H2 (600 meV)
5% dosed - bkgd
pure C2H2 - bkgd
pure - 5%
S(Q,ω) / Arb. units
2000
2500
3000
3500
4000
Wavenumber / cm-1
(b)
Au(2%)/C + C2H2 (250 meV)
5% dosed - bkgd
pure C2H2 - bkgd
pure - 5%
S(Q,ω) / Arb. units
800
1200
1600
Wavenumber / cm-1

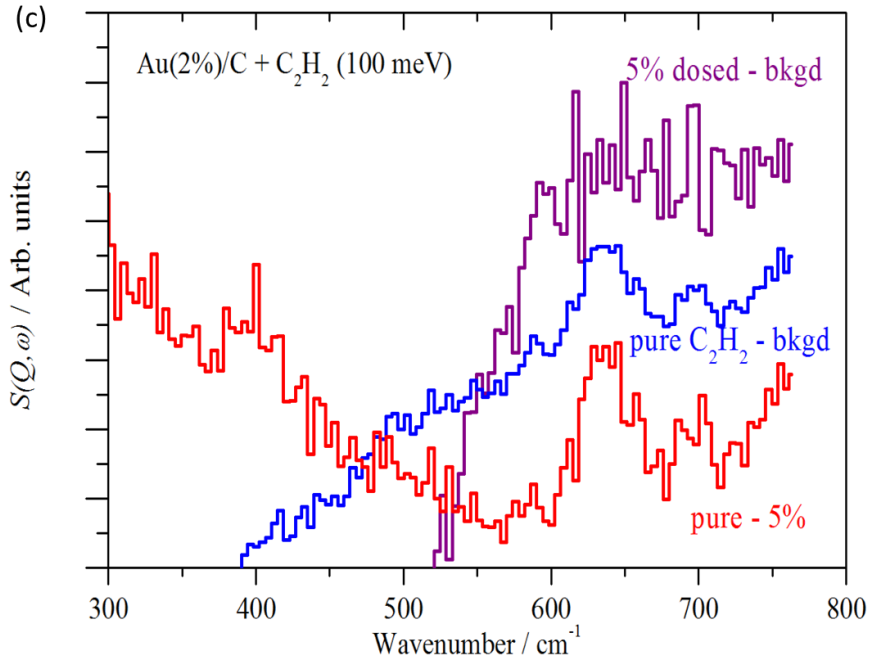

Figure 10. INS difference spectra obtained from the 2wt % Au/C-AR catalyst in: **(a)** the C–H/O–H stretch region; **(b)** the C–H in-plane bend and C–C stretch region and (c) the C–H out-of-plane bend region.

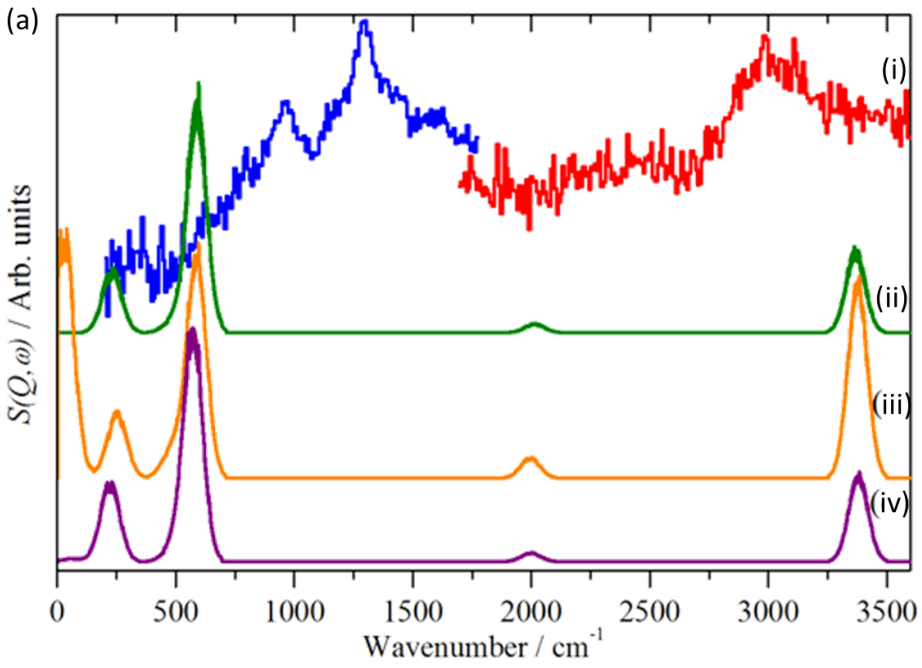

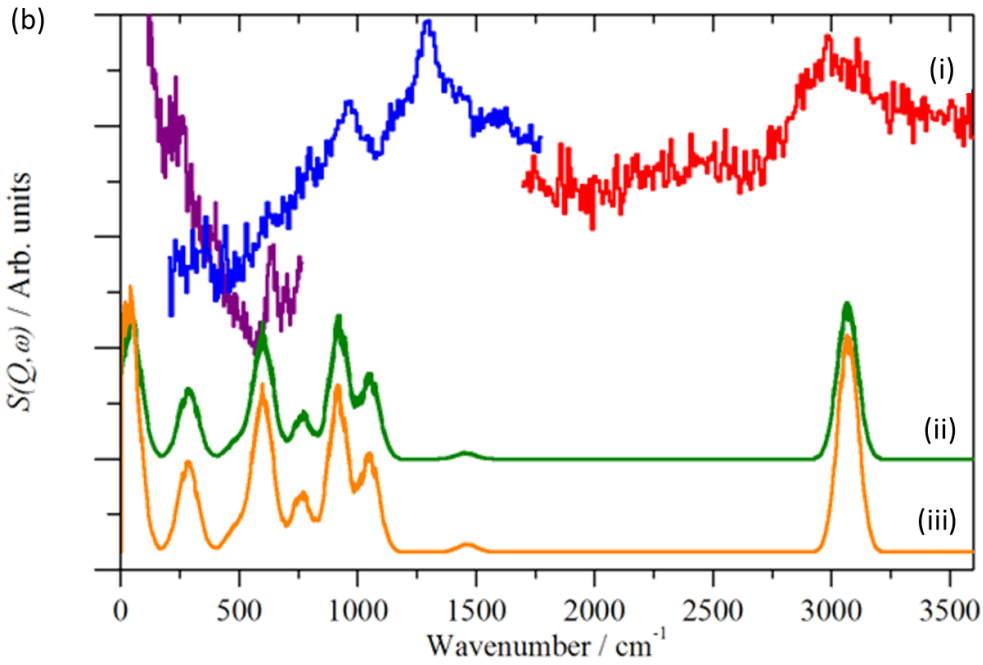

Figure 11. (a) Comparison of INS spectrum of: (i) (C_2H_2 (100%) dosed – C_2H_2 (5%) dosed) with those calculated for gold acetylide as: (ii) an isolated molecule, (iii) a molecule adsorbed in the on-top site on graphene and (iv) a molecule adsorbed in the six-fold site on graphene. **(b)** Comparison of INS spectrum of: (i) (C_2H_2 (100%) dosed – C_2H_2 (5%) dosed) with those calculated for $Au_4C_2H_2$ as: (ii) an isolated molecule and (iii) a molecule adsorbed on graphene.

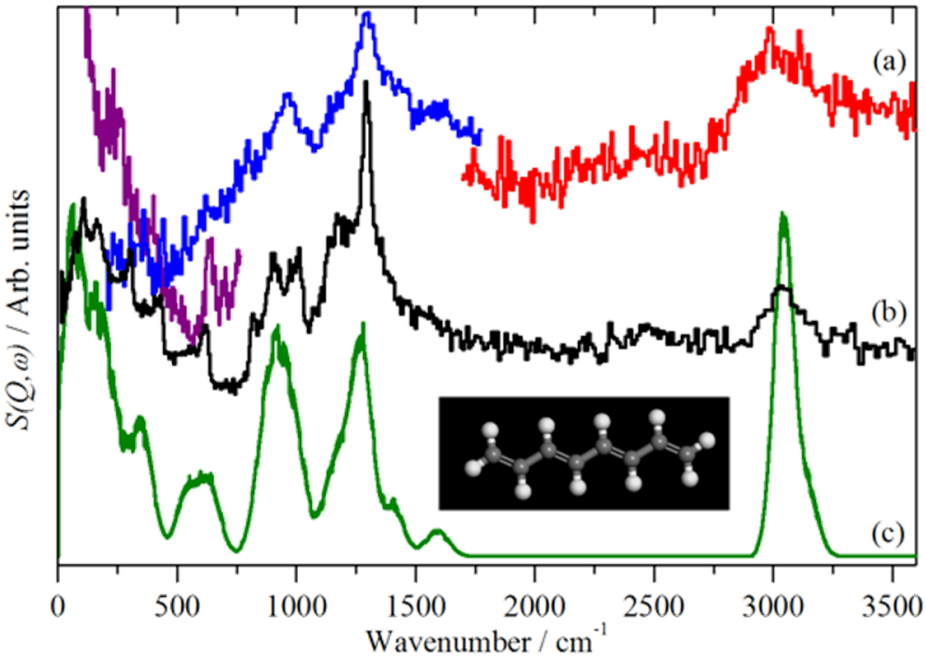

Figure 12. Comparison of INS spectrum of: (a) (C_2H_2 (100%) dosed – C_2H_2 (5%) dosed) with (b) polyacetylene[36] recorded on a TOSCA-like INS spectrometer and (c) that calculated for all-trans-1,3,5,7-octatetraene. The inset shows the idealised structure of all-trans-1,3,5,7-octatetraene.

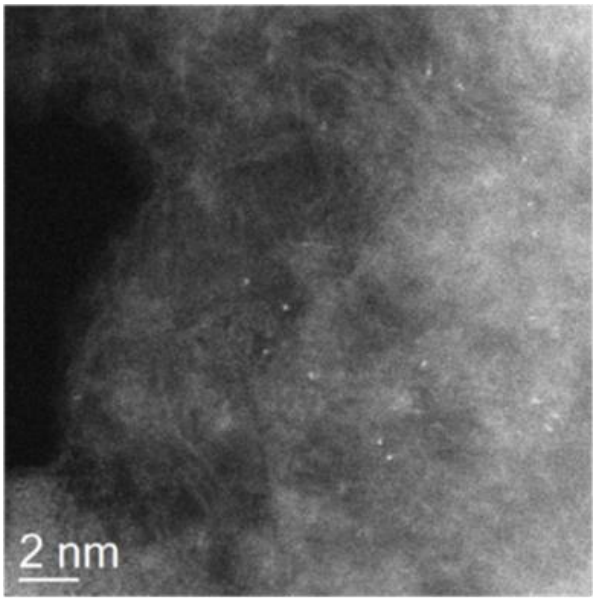

Figure 13. HAADF-STEM images of the 2wt % Au/C-AR catalyst after use showing atomically dispersed Au entities.

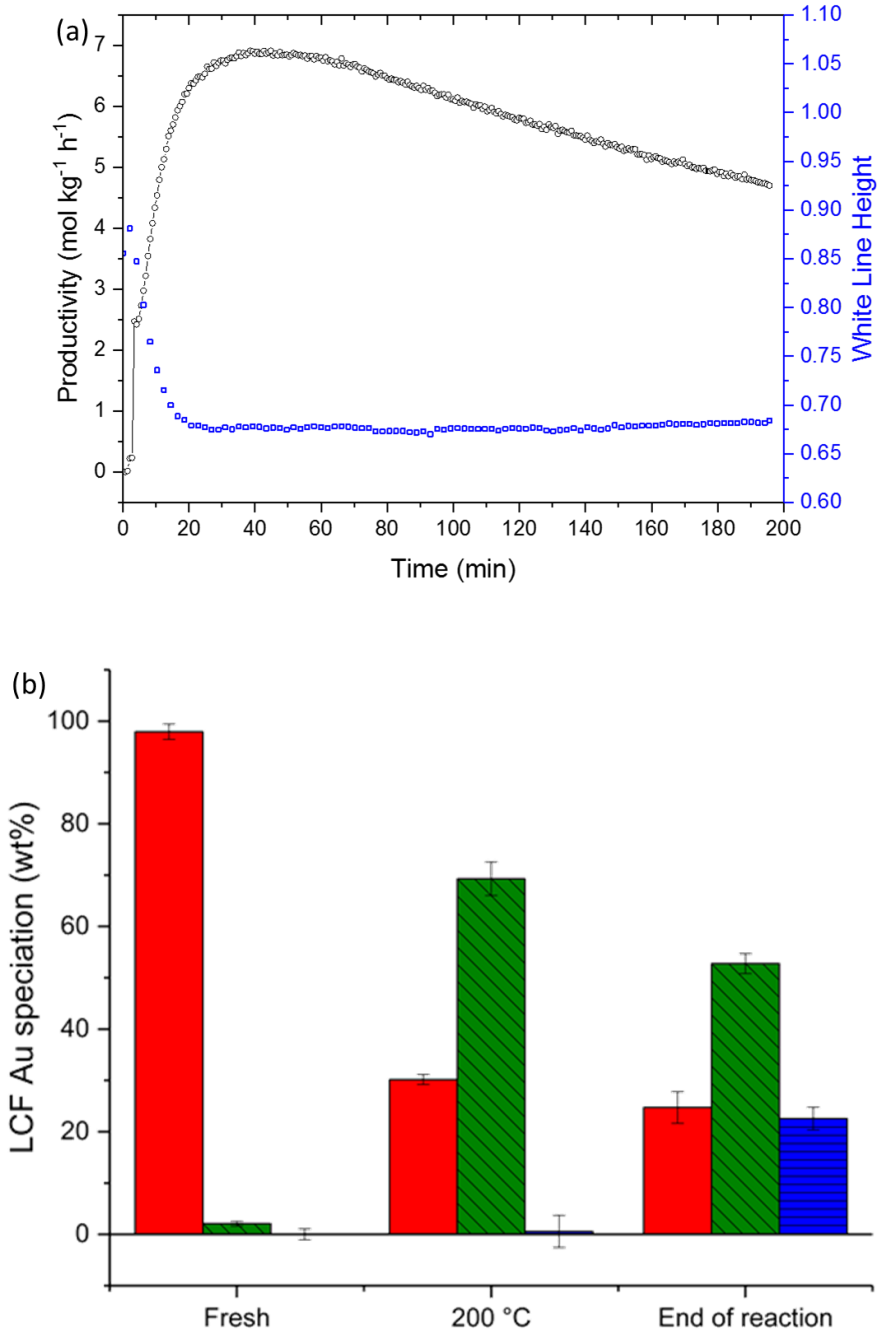

Figure 14. **(a)** VCM productivity of the 2wt % Au/C-AR catalyst during the first 200 min of reaction combined with *in situ* Au L_3-edge XANES analysis. The open black circles represent VCM production as a function of time-on-line. The simultaneously acquired normalized white line data (blue open squares) from XANES analysis are also shown. **(b)** Linear combination fitting for the fresh 2wt %Au/C-AR catalyst as prepared at room temperature, once it had reached 200 ˚C under Ar and at the end of the reaction (after 350 min). The percentage of Au associated with; Au(I) chloride (standard $[AuCl_2]^-$) is

shown in *red*, Au(III) chloride (standard $KAuCl_4$) is shown in *green* and Au(0) metal (standard Au foil) is shown in *blue*.

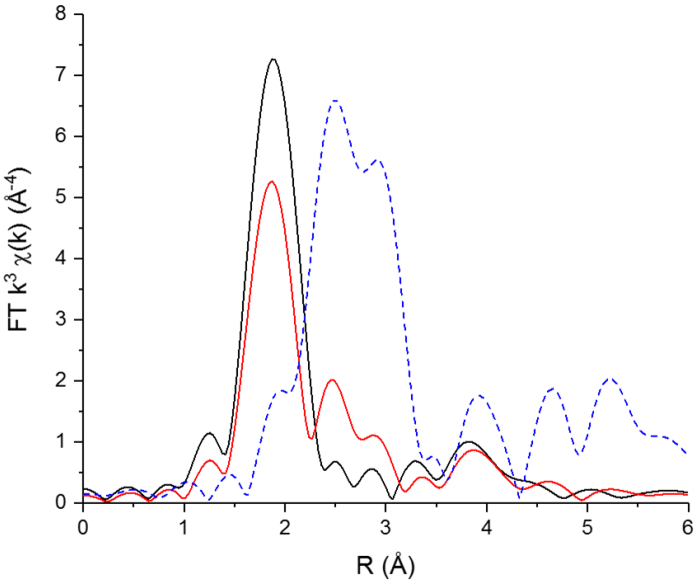

Figure 15. Magnitude of Fourier Transform (FT) of extended X-ray absorption spectra k^3 weighted from the 2wt % Au/C-AR catalyst in the 'as prepared state' and 'used state' (after 350 min of reaction). *Black line*; FT of the fresh catalyst: *red line;* FT of the catalyst after 350 min of reaction: *blue line*; FT of the reference material gold foil.

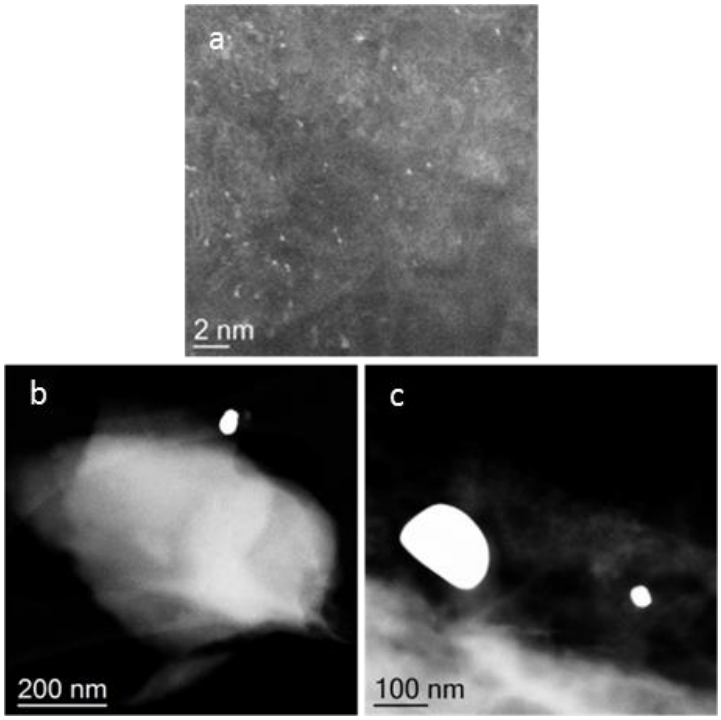

Figure 16. HAADF-STEM images of the 2wt % Au/C-AR catalyst after use. In the material after use a mixture of (a) atomically dispersed Au entities and (b,c) larger Au particles were observed.

For Table of Contents Only

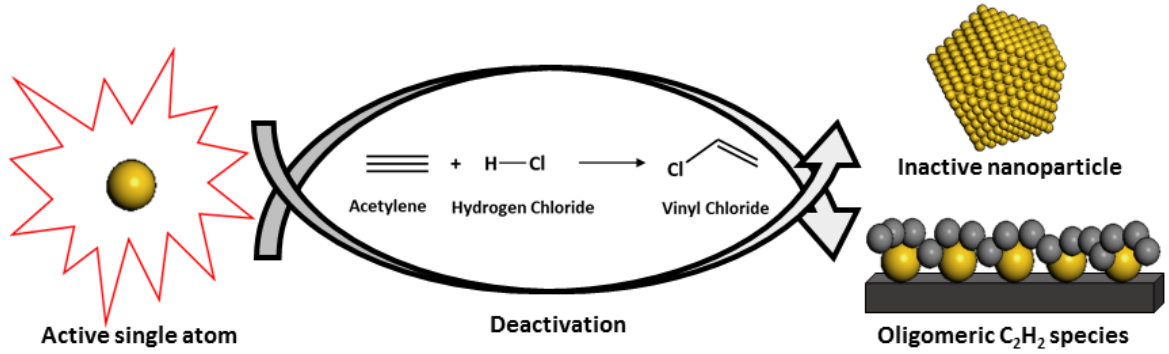

REFERENCES

(1) Agnew, J. B.; Shankar, H. S. Catalyst Deactivation in Acetylene Hydrochlorination. *Ind. Eng. Chem. Prod. Res. Dev.* **1986**, *25* (1), 19–22.

(2) Bremer, H.; Lieske, H. Kinetics of the Hydrochlorination of Acetylene on $HgCl_2$/Active Carbon Catalysts. *Appl. Catal.* **1985**, *18* (1), 191–203.

(3) Hutchings, G. J.; Grady, D. T. Effect of Drying Conditions on Carbon Supported Mercuric Chloride Catalysts. *Appl. Catal.* **1985**, *16* (3), 411–415.

(4) Hutchings, G. J.; Grady, D. T. Hydrochlorination of Acetylene: The Effect of Mercuric Chloride Concentration on Catalyst Life. *Appl. Catal.* **1985**, *17* (1), 155–160.

(5) Hutchings, G. J. Vapor Phase Hydrochlorination of Acetylene: Correlation of Catalytic Activity of Supported Metal Chloride Catalysts. *J. Catal.* **1985**, *96* (1), 292–295.

(6) Johnston, P.; Carthey, N.; Hutchings, G. J. Discovery, Development, and Commercialization of Gold Catalysts for Acetylene Hydrochlorination. *J. Am. Chem. Soc.* **2015**, *137* (46), 14548–14557.

(7) Conte, M.; Carley, A. F.; Heirene, C.; Willock, D. J.; Johnston, P.; Herzing, A. A.; Kiely, C. J.; Hutchings, G. J. Hydrochlorination of Acetylene Using a Supported Gold Catalyst: A Study of the Reaction Mechanism. *J. Catal.* **2007**, *250* (2), 231–239.

(8) Liu, X.; Conte, M.; Elias, D.; Lu, L.; Morgan, D. J.; Freakley, S. J.; Johnston, P.; Kiely, C. J.; Hutchings, G. J. Investigation of the Active Species in the Carbon-Supported Gold Catalyst for Acetylene Hydrochlorination. *Catal. Sci. Technol.* **2016**, *6* (13), 5144–5153.

(9) Malta, G.; Kondrat, S. A.; Freakley, S. J.; Davies, C. J.; Lu, L.; Dawson, S.; Thetford, A.; Gibson, E. K.; Morgan, D. J.; Jones, W.; Wells, P. P.; Johnston, P.; Catlow, C. R. A.; Kiely, C. J.; Hutchings, G. J. Identification of Single-Site Gold Catalysis in Acetylene Hydrochlorination. *Science* **2017**, *355* (6332), 1399–1403.

(10) Fong, Y. Y.; Visser, B. R.; Gascooke, J. R.; Cowie, B. C. C.; Thomsen, L.; Metha, G. F.; Buntine, M. A.; Harris, H. H. Photoreduction Kinetics of Sodium Tetrachloroaurate under Synchrotron Soft X-Ray Exposure. *Langmuir* **2011**, *27* (13), 8099–8104.

(11) Ozkaraoglu, E.; Tunc, I.; Suzer, S. X-Ray Induced Reduction of Au and Pt Ions on Silicon Substrates. *Surf. Coatings Technol.* **2007**, *201* (19–20 SPEC. ISS.), 8202–8204.

(12) Ozkaraoglu, E.; Tunc, I.; Suzer, S. Preparation of Au and Au-Pt Nanoparticles within PMMA Matrix Using UV and X-Ray Irradiation. *Polymer* **2009**, *50* (2), 462–466.

(13) Karadas, F.; Ertas, G.; Ozkaraoglu, E.; Suzer, S. X-Ray-Induced Production of Gold Nanoparticles on a SiO2/Si System and in a Poly(Methyl Methacrylate) Matrix. *Langmuir* **2005**, *21* (1), 437–442.

(14) Kitagawa, H.; Kojima, N.; Matsushita, N.; Ban, T.; Tsujikawa, I. Studies of Mixed-Valence States in Three-Dimensional Halogen-Bridged Gold Compounds, $Cs_2Au^{I}Au^{III}X_6$(X = Cl, Br or I). Part 1. Synthesis, X-Ray Powder Diffraction, and Electron Spin Resonance Studies of $CsAu_{0.6}Br_{2.6}$. *J. Chem. Soc. Dalt. Trans.* **1991**, *0* (11), 3115–3119.

(15) Kitagawa, H.; Kojima, N.; Nakajima, T. Studies of Mixed-Valence States in Three-Dimensional Halogen-Bridged Gold Compounds, $Cs_2Au^{I}Au^{III}X_6$, (X = Cl, Br or I). Part 2. X-Ray Photoelectron Spectroscopic Study. *J. Chem. Soc. Dalt. Trans.* **1991**, *0* (11), 3121-3125.

(16) Nkosi, B.; Adams, M. D.; Coville, N. J.; Hutchings, G. J. Hydrochlorination of Acetylene Using Carbon-Supported Gold Catalysts: A Study of Catalyst Reactivation. *J. Catal.* **1991**, *128* (2), 378–386.

(17) Dai, B.; Wang, Q.; Yu, F.; Zhu, M. Effect of Au Nano-Particle Aggregation on the Deactivation of the $AuCl_3$/AC Catalyst for Acetylene Hydrochlorination. *Sci. Rep.* **2015**, *5* (April), 10553.

(18) Zhang, H.; Dai, B.; Wang, X.; Li, W.; Han, Y.; Gu, J.; Zhang, J. Non-Mercury Catalytic Acetylene Hydrochlorination over Bimetallic Au–Co(III)/SAC Catalysts for Vinyl Chloride Monomer Production. *Green Chem.* **2013**, *15* (3), 829.

(19) Zhu, M.; Wang, Q.; Chen, K.; Wang, Y.; Huang, C.; Dai, H.; Yu, F.; Kang, L.; Dai, B. Development of a Heterogeneous Non-Mercury Catalyst for Acetylene Hydrochlorination. *ACS Catal.* **2015**, *5* (9), 5306–5316.

(20) Nkosi, B.; Coville, N. J.; Hutchings, G. J.; Adam, M.D.; Friedl, J. Hydrochlorination of Acetylene Using Gold Catalysts: A Study of Catalyst Deactivation. *J. Catal.* **1991**, *128* (2), 366–377.

(21) Friedl, J.; Wagner, F. E.; Nkosi, B.; Towert, M.; Coville, N. J.; Adams, M. D.; Hutchings, G. J. ^{197}Au Mössbauer Study of the Deactivation and Reactivation of a Carbon-Supported AuCl4 - Hydrochlorination Catalyst. *Hyperfine Interact.* **1992**, *69* (1–4), 767–770.

(22) Conte, M.; Carley, A. F.; Hutchings, G. J. Reactivation of a Carbon-Supported Gold Catalyst for the Hydrochlorination of Acetylene. *Catal. Letters* **2008**, *124* (3–4), 165–167.

(23) Conte, M.; Davies, C. J.; Morgan, D. J.; Davies, T. E.; Carley, A. F.; Johnston, P.; Hutchings, G. J. Modifications of the Metal and Support during the Deactivation and Regeneration of Au/C Catalysts for the Hydrochlorination of Acetylene. *Catal. Sci. Technol.* **2013**, *3* (1), 128–134.

(24) Nkosi, B.; Coville, N. J.; Hutchings, G. J. Reactivation of a Supported Gold Catalyst for Acetylene Hydrochlorination. *J. Chem. Soc. Chem. Commun.* **1988**, *0* (1), 71-72.

(25) Pouwer, R. H.; Williams, C. M.; Raine, A. L.; Harper, J. B. "One-Step" Alkynylation of Adamantyl Iodide with Silver(I) Acetylides. *Org. Lett.* **2005**, *7* (7), 1323–1325.

(26) Pouwer, R. H.; Harper, J. B.; Vyakaranam, K.; Michl, J.; Williams, C. M.; Jessen, C. H.; Bernhardt, P. V. Investigating Direct Alkynylation at the Bridgehead of Bicyclic Cages Using Silver(I) Acetylides. *European J. Org. Chem.* **2007**, *2007* (2), 241–248. .

(27) Han, F.; Li, J.; Zhang, H.; Wang, T.; Lin, Z.; Xia, H. Reactions of Osmabenzene with Silver/Copper Acetylides: From Metallabenzene to Benzene. *Chem. - A Eur. J.* **2015**, *21* (2), 565–567.

(28) Castro, C. E.; Havlin, R.; Honwad, V. K.; Malte, A.; Moje, S. Copper(I) Substitutions. Scope and Mechanism of Cuprous Acetylide Substitutions. *J. Am. Chem. Soc.* **1969**, *91* (23), 6464–6470.

(29) Bertus, P.; Fécourt, F.; Bauder, C.; Pale, P. Evidence for the in Situ Formation of Copper Acetylides during Pd/Cu Catalyzed Synthesis of Enynes: A New Synthesis of Allenynols. *New J. Chem.* **2004**, *28* (1), 12–14.

(30) Simonneau, A.; Jaroschik, F.; Lesage, D.; Karanik, M.; Guillot, R.; Malacria, M.; Tabet, J.-C.; Goddard, J.-P.; Fensterbank, L.; Gandon, V.; Gimbert, Y. Tracking Gold Acetylides in Gold(I)-Catalyzed Cycloisomerization Reactions of Enynes. *Chem. Sci.* **2011**, *2* (12), 2417-2422.

(31) Hashmi, A. S. K. Gold-Catalyzed Organic Reactions Gold-Catalyzed Organic Reactions. *Chem. Rev.* **2007**, *107*, 3180–3211.

(32) Li, Z.; Brouwer, C.; He, C. Gold-Catalyzed Organic Transformations. *Chem. Rev.* **2008**, *108* (8), 3239–3265.

(33) Schmidbaur, H.; Schier, A. Gold η^2-Coordination to Unsaturated and Aromatic Hydrocarbons: The Key Step in Gold-Catalyzed Organic Transformations. *Organometallics* **2010**, *29* (1), 2–23.

(34) Corma, A.; Leyva-Pérez, A.; Sabater, M. J. Gold-Catalyzed Carbon-Heteroatom Bond-Forming Reactions. *Chem. Rev.* **2011**, *111* (3), 1657–1712.

(35) Hirata, S.; Torii, H.; Furukawa, Y.; Tasumi, M.; Tomkinson, J. Inelastic Neutron Scattering from Trans-Polyacetylene. *Chem. Phys. Lett.* **1996**, *261* (3), 241–245.

(36) Ravel, B.; Newville, M. ATHENA, ARTEMIS, HEPHAESTUS: Data Analysis for X-Ray Absorption Spectroscopy Using IFEFFIT. *J. of Synchrotron Rad.* **2005**, *12*, 537–541.

(37) Newville, M. IFEFFIT: Interactive XAFS Analysis and FEFF Fitting. *J. Synchrotron Rad.* **2001**, *8* (2), 322–324.

(38) Bewley, R. I.; Eccleston, R. S.; McEwen, K. A.; Hayden, S. M.; Dove, M. T.; Bennington, S. M.; Treadgold, J. R.; Coleman, R. L. S. MERLIN, a New High Count Rate Spectrometer at ISIS. *Phys. B Condens. Matter* **2006**, *385–386*, 1029–1031.

(39) Sheppard, N.; De La Cruz, C. Vibrational Spectra of Hydrocarbons Adsorbed on Metals. Part II. Adsorbed Acyclic Alkynes and Alkanes, Cyclic Hydrocarbons Including Aromatics and Surface

Hydrocarbon Groups Derived from the Decomposition of Alkyl Halides, Etc. *Adv. Catal.* **1998**, *42*, 181–313.

(40) Dymkowski, K.; Parker S. F.; Fernandez-Alonso F.; Mukhopadhyay S. AbINS: The Modern Software for INS Interpretation. *Physica B* (**2018**) [*doi:* 10.1016/j.physb.2018.02.034].